Hindawi
Mathematical Problems in Engineering
Volume 2018, Article ID 1295986, 14 pages
https://doi.org/10.1155/2018/1295986

Research Article

Analytical Model of Wave Loads and Motion Responses for a Floating Breakwater System with Attached Dual Porous Side Walls

Weiliang Qiao,[1] **Keh-Han Wang**,[2] **Wenqi Duan**,[1] **and Yuqing Sun**[1]

[1]*Marine Engineering College, Dalian Maritime University, Dalian 116026, China*
[2]*Dept. of Civil and Environmental Engineering, Univ. of Houston, Houston, TX 77024, USA*

Correspondence should be addressed to Weiliang Qiao; qiao_wl@hotmail.com

Received 17 September 2018; Accepted 6 November 2018; Published 19 November 2018

Academic Editor: Roman Lewandowski

A set of two-dimensional analytical solutions considering the effects of diffraction and radiation are presented in this study to investigate the hydrodynamic interaction between an incident linear wave and a proposed floating breakwater system consisting of a rectangular-shaped body and two attached vertical side porous walls in an infinite fluid domain with finite water depth. The Matched Eigenfunction Expansion Method (MEEM) for multiple fluid domains is applied to derive theoretically the velocity potentials and associated unknown coefficients for wave diffraction and body motion induced radiation in each subdomain. Also, the exciting forces, as well as the added mass and damping coefficients for the floating breakwater system under the surge, heave, and pitching motions, are formulated. The displacements of breakwater motions are determined by solving the equation of motion. As a verification of the analytical model, the present solutions of the limiting cases in terms of exciting forces, moments, added masses, and damping coefficients are found to be well matched with other published numerical results. Additionally, the hydrodynamic performances and the dynamic responses in terms of Response Amplitude Operators (RAOs) of the proposed floating breakwater system are evaluated versus various dimensionless variables, such as wavelength and porous-effect parameter. The results show that the attached porous walls with selected porous properties are observed to have the advantages of reducing wave impacts on the floating breakwater system and at the same time its dynamic responses are also noticeably improved.

1. Introduction

The ocean-oriented activities, such as oil and gas extraction, aquacultural production, and recreations, have been identified to generate tremendous values to humans. Protection of the shoreline structures or offshore production facilities by degradation of the wave-structure interaction is therefore a vital issue in the coastal and offshore engineering applications. Various artificial structures have been designed and optimized for this purpose, of which the floating breakwaters or barriers are considered as valuable alternatives to conventional fixed gravity-type breakwaters [1]. The performance optimization of a breakwater, especially the type of floating breakwater, has received much attention with the advantage of energy dissipation [2]. Additionally, the porous structures may provide an added alternative to improve the performance of floating breakwaters.

Hydrodynamic analysis is widely applied to examine the wave-reduction performance of a floating breakwater. Mei and Black [3] investigated the wave forces acting on the rectangular floating obstacles by the variational-formulation-based numerical approach. Later, the wave radiation induced by small oscillations of a floating body was also studied [4]. A simplified analytical model to estimate the hydrodynamic performance of a long rectangular floating breakwater was developed under the assumption of a small gap condition [5]. Also, the diffraction and radiation problem of a rectangular buoy were analyzed under the conditions of heave oscillation [6], as well as in three dimensional scale, the sway, heave, and rolling motions [7]. Damping mechanisms of a floating breakwater were investigated numerically and experimentally considering the cases of a regular pontoon, a regular pontoon with wing plates attached, and a regular pontoon with wing plates penetrated [8]. Additionally, the hydrodynamic

performances of rectangular boxes of fixed single and fixed double subject to the heave motion were estimated under the actions of either regular or irregular water waves [9]. Later, the wave absorbing effectiveness of different types of floating breakwaters, such as single box, double boxes, or board net, was also investigated [10].

Due to the advantage of energy dissipation, the water-wave absorbing phenomena have been observed when waves pass through a porous medium; that is, a porous structure can effectively attenuate both reflected and transmitted waves. Following the porous wavemaker theory of Chwang [11], considerable studies related to the interaction between porous structures and water waves were performed theoretically and experimentally, especially the porous barriers or the porous structures attached to the floating breakwaters. The wave energy dissipation of thin permeable wall was verified by conducting sets of experiments [12]. Analytical approaches have been carried out by Manam and Sivanesan [13] and Chwang and Dong [14], as well as Zhu and Chwang [15], to study the reflection and transmission problem of water waves propagating past vertical porous barriers. The hydroelastic issues between gravity waves and a submerged horizontal flexible porous plate were investigated by Behera and Sahoo [16]. The studies of perforated wall breakwaters and dual submerged horizontal porous plates were given in [17, 18], respectively. In order to examine the effectiveness of wave absorption by porous plates, the interactions between different types of porous plates and oblique monochromatic waves were investigated by Cho and Kim [19]. The concept of porous barrier was extended by Wang and Ren [20, 21] to analytically study the interaction between water waves and a flexible porous breakwater or, in a three-dimensional domain, a concentric porous cylinder system. The diffraction problems of either a circular porous plate submerged horizontally or a system with dual circular porous plates were investigated based on the linear potential flow theory [22, 23]. Recently, the scattering of water waves by a rectangular floating body that attached with two vertically porous walls was investigated analytically and experimentally by Qiao et al. [24]. In practices, the types of porous structure are various depending on the requirements of engineering problem; however, single or several vertical porous plates (including barrier and circular) and porous cylinder are the most common in engineering field. The vertical porous plates were often employed to absorb waves to protect coastal [25, 26]; furthermore, a set of porous plates were placed at the bottom of a wave tank to absorb waves [27]. The porous cylinder was employed to protect structure in Trafalgar offshore windfarm [28]; almost for the same purpose, a concentric two-cylinder system, involving an interior impermeable cylinder and external porous cylinder, was designed for Ekofisk gravity offshore structure in the North Sea [29]; then, the concept of single-layered porous cylinder was extended to double-layered perforated cylinder by Xiao et al. [30], and the experiments were conducted to investigate the hydrodynamic performances.

To achieve the combination of the advantages of a floating body and porous wall features, a new breakwater system that consists of a partially submerged pontoon-like body and two attached porous side walls is proposed in this study to provide a protected region sheltering from wave action. The results of wave reflection/transmission and wave induced hydrodynamic loads under the condition that the breakwater system is in a fixed position were given in Qiao et al. [24]. The investigation of wave interactions with the breakwater system is further extended to include the effect of the induced motions of the floating breakwater system, the so-called radiation problem. Under the assumptions of linear incident waves and small translational and rotational motions of surge, heave, and pitch, this study focuses on the investigation of hydrodynamic coefficients, such as the added mass and damping coefficient, and the dynamic responses of the floating breakwater system through developing an analytical model with solutions of diffracted and radiated waves and the equation of motion which is formulated and solved. The solutions of the velocity potentials in the defined regions, including the diffraction and radiation velocity potentials, are obtained by solving the formulated governing equations as well as the boundary and matching conditions. To verify the analytical solutions derived from this study, some limited numerical results published in literatures were adopted for comparisons. Additionally, the effects of the incident wave parameters and porous walls conditions on the hydrodynamic coefficients and RAOs (Response Amplitude Operators) are examined and discussed.

2. Theoretical Formulations and Solutions

The problem statement as illustrated in Figure 1 shows a train of right-going, small-amplitude, Airy waves with the frequency ω, wave height H, and wave length λ to interact normally with a floating breakwater system that consists of a partially submerged rectangular structure and two attached fully submerged side porous walls. Subject to the wave induced hydrodynamic loads, the breakwater system responds with two translational motions and one rotational motion, i.e., surge, heave, and pitching motions. The Cartesian coordinates system is employed to define this two-dimensional boundary value problem. The x-axis is along the still water surface, where $x = 0$ is set at the center of the floating breakwater system, and the z-axis points vertically upwards with an origin located at the still water surface. The rectangular structure with a length of $2a$ and a submergence of s is initially positioned in a domain with undisturbed constant water depth h. Both of the thin porous walls have a length of d-s.

In this study, the fluid is assumed to be incompressible and inviscid and the motion irrational. Subsequently, the potential flow theory, providing that the velocity potential satisfies the Laplace Equation, with the defined boundary conditions could be applied to solve the waves and breakwater interaction problem. As shown in Figure 1, the entire fluid domain is divided into three subdomains, namely, regions I, II, and III, respectively. Region I is the subdomain upstream of the breakwater system ($x \le a,\ -h \le z \le 0$); region II is the subdomain between the two porous walls ($-a \le x \le a,\ -d \le z \le -s$); and region III is the subdomain downstream of the breakwater system ($a \le x,\ -h \le z \le 0$). In the fluid domain,

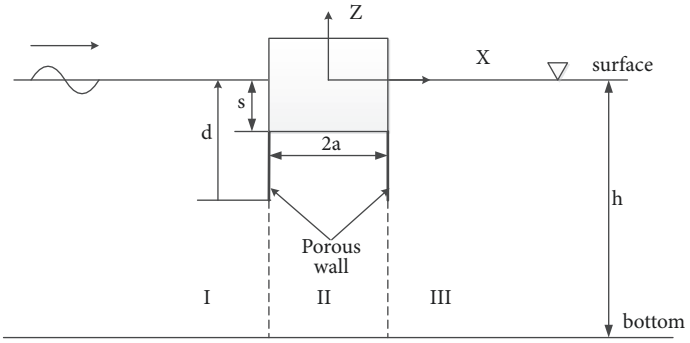

Figure 1: Schematic diagram of a floating body with attached two porous walls under the action of an incident wave and forced surge, heave, and pitching motions.

the Laplace equation of a complete velocity potential serves as the basic equation to describe the fluid motion, namely,

$$\nabla^2\phi = 0; \tag{1}$$

The fluid velocity potential ϕ includes three components, incident wave potential ϕ_I, diffracted wave potential ϕ_D, and the radiated wave potential Φ_R, which covers the induced motions of the floating breakwater system. In this study, the dynamic motions of surge, heave, and pitching are considered. Thus, the velocity potential ϕ can be expressed as

$$\phi = \phi_I + \phi_D + \sum_{j=1}^{3}\Phi_R^{(L)} \tag{2}$$

where the subscript L = 1, 2, 3 donates the surge, heave, and pitching motions of the breakwater system, respectively. In this study, the incident wave potential is given as

$$\phi_I = -\mathrm{i}\frac{gH}{2\omega}e^{\mathrm{i}k_0(x+a)}\frac{\cosh k_0(z+h)}{\cosh k_0 h}e^{-\mathrm{i}\omega t} \tag{3}$$

where k_0 is the wave number, ω is the wave frequency, and g is the gravitational acceleration. Here, k_0 and ω satisfy the usual dispersion relation

$$\omega^2 = gk_0\tanh(k_0 h) \tag{4}$$

2.1. Theoretical Formulations and Solutions of the Incident and Diffracted Velocity Potentials. To solve the wave radiation problem in a linear wave system, the wave induced hydrodynamic forces and moment according to the wave diffraction approach by assuming the body is in a fixed position are required to be determined priorly. The wave diffraction solutions for the proposed breakwater system with two attached porous walls have been obtained in a previous study given in Qiao et al. [24] and Yip and Chwang [31]. Here, only limited formulations and solutions are summarized below. Let us define the wave diffraction potentials as ϕ_{Di}; $i = 1, 2, 3$ stands for the subdomains I, II, and III, respectively. The Laplace equations of ϕ_{Di} can be solved with the uses of the linearized kinematic and dynamic free surface boundary condition, bottom boundary condition, no flow condition at the body surface, and matching conditions at the interfaces of porous wall locations, including the porous flow conditions expressed as (Chwang [11])

$$\frac{\partial\phi_{D1}}{\partial x} = \frac{\partial\phi_{D2}}{\partial x} = \frac{b_1}{\mu}(p_{D1} - p_{D2}) \quad at\ x = -a,\ -d \le z \le -s \tag{5}$$

$$\frac{\partial\phi_{D3}}{\partial x} = \frac{\partial\phi_{D2}}{\partial x} = \frac{b_2}{\mu}(p_{D2} - p_{D3}) \quad at\ x = -a,\ -d \le z \le -s \tag{6}$$

where b_1 and b_2, having the dimension of length, are, respectively, material constants for the porous walls A and B, p_{Di} (i=1, 2, 3) are the dynamic pressures induced by the incident and diffracted velocity potentials, and μ is the dynamic viscosity of the fluid. The wave diffraction solutions are derived as

$$\phi_{D1} = \sum_{m=0}^{\infty}\left[I_m e^{\widetilde{k}_m(x+a)} + F_m e^{-\widetilde{k}_m(x+a)}\right]\frac{\cos\widetilde{k}_m(z+h)}{\cos\widetilde{k}_m h} \cdot e^{-\mathrm{i}\omega t} \tag{7}$$

$$\phi_{D2} = (C_0 x + E_0)e^{-\mathrm{i}\omega t} + \sum_{m=1}^{\infty}\left[C_m\frac{\cosh(r_m x)}{\cosh(r_m a)} + E_m\frac{\sinh(r_m x)}{\sinh(r_m a)}\right] \cdot \cos r_m(z+h)e^{-\mathrm{i}\omega t} \tag{8}$$

$$\phi_{D3} = \sum_{\mathrm{m}=0}^{\infty}\left[T_m e^{\widetilde{k}_m(x-a)}\right]\frac{\cos\widetilde{k}_m(z+h)}{\cos\widetilde{k}_m h}e^{-\mathrm{i}\omega t} \tag{9}$$

where F_m, C_m, E_m, and T_m ($m = 0, 1, 2, 3, \ldots$) are unknown complex coefficients to be determined. $I_m, \widetilde{k}_m$, and r_m ($m = 0, 1, 2, 3, \ldots$) are expressed separately as

$$I_m = \left\{-\mathrm{i}\frac{gH}{2\omega}, 0, 0, 0, \ldots\ \ldots\right\} \tag{10}$$

$$\widetilde{k}_m = \{\mathrm{i}k_0, -k_1, -k_2, -k_3, \ldots\ \ldots, -k_m, \ldots\ \ldots\} \tag{11}$$

$$r_m = \frac{m\pi}{h-s} \tag{12}$$

Here, k_m can be calculated from

$$\omega^2 = -gk_m \tanh\left(k_m h\right) \tag{13}$$

Substituting (7), (8), and (9) into the following derived matching equations

$$\int_{-h}^{0} \frac{\partial \phi_{D1}}{\partial x} \cos \widetilde{k}_n (z+h)\, dz = \int_{-h}^{-s} \frac{\partial \phi_{D2}}{\partial x} \cos \widetilde{k}_n (z+h)\, dz; \quad x = -a \ \ (n = 0, 1, 2, 3, \ldots) \tag{14}$$

$$\int_{-h}^{0} \frac{\partial \phi_{D3}}{\partial x} \cos \widetilde{k}_n (z+h)\, dz = \int_{-h}^{-s} \frac{\partial \phi_{D2}}{\partial x} \cos \widetilde{k}_n (z+h)\, dz; \quad x = -a \ \ (n = 0, 1, 2, 3, \ldots) \tag{15}$$

$$\int_{-h}^{-d} \phi_{D1} \cos r_n (z+h)\, dz + \int_{-d}^{-s} \widetilde{\phi}_{D1} \cos r_n (z+h)\, dz = \int_{-h}^{-s} \phi_{D2} \cos r_n (z+h)\, dz; \quad x = -a, \ \ (n = 0, 1, 2 \ldots) \tag{16}$$

$$\int_{-h}^{-d} \phi_{D3} \cos r_n (z+h)\, dz + \int_{-d}^{-s} \widetilde{\phi}_{D3} \cos r_n (z+h)\, dz = \int_{-h}^{-s} \phi_{D2} \cos r_n (z+h)\, dz; \quad x = -a, \ \ (n = 0, 1, 2 \ldots) \tag{17}$$

and utilizing the orthogonality properties of solution eigenfunctions, the unknown coefficients C_n, D_n, R_n, T_n $(n = 0, 1, 2, 3, \ldots, M)$ for the diffraction potentials can be determined by solving the 4(M+1) system of algebraic equations. Here, the terms with summation of infinite series are approximated by a large but finite number of M terms. In (16) and (17), $\widetilde{\phi}_{D1}$ and $\widetilde{\phi}_{D3}$ are given as

$$\widetilde{\phi}_{D1} = \sum_{m=0}^{\infty} \left[\left(I_m + F_m\right) - \frac{\widetilde{k}_m}{\mathrm{i}G_{01}k_0} \left(I_m - F_m\right) \right] \cdot \frac{\cos \widetilde{k}_m (z+h)}{\cos \widetilde{k}_m h} \tag{18}$$

$$\widetilde{\phi}_{D3} = \sum_{m=0}^{\infty} \left(1 + \frac{\widetilde{k}_m}{\mathrm{i}G_{01}k_0} \right) T_m \frac{\cos \widetilde{k}_m (z+h)}{\cos \widetilde{k}_m h} \tag{19}$$

where $G_{01} = \rho\omega b_1/(\mu k_0)$ and $G_{02} = \rho\omega b_2/(\mu k_0)$ are dimensionless parameters defined according to Chwang [11] to represent the porous effect parameters of porous walls A and B, respectively.

2.2. Theoretical Formulations of the Radiated Velocity Potentials. For the radiation problem, the displacements of the floating breakwater system in motion are given as

$$X_j = X_{0j} e^{-\mathrm{i}\omega t} \quad j = 1, 2, 3 \tag{20}$$

where X_{oj} $(j = 1, 2, 3)$ are the amplitudes of surge, heave, and pitching motions, respectively. Let $\phi_{Ri}^{(L)}$ $(L = 1, 2, 3; i = 1, 2, 3)$ be the spatial radiated potentials describing the small-amplitude oscillations, where L^{th} indices denote, respectively, the induced surge, heave, and pitching motions while the i^{th} indices represent the subdomains of I, II, and III, respectively. Then, the total radiated potentials in any of the flow domains can be expressed as

$$\Phi_R^{(L)} = X_j \phi_R^{(L)} = \mathrm{Re}\left[-\mathrm{i}\omega X_{0j} \phi_R^{(L)} (x, z)\, e^{-\mathrm{i}\omega t} \right] \tag{21}$$

As the velocity potentials $\phi_R^{(L)}$ satisfy the Laplace equation, we have

$$\nabla^2 \phi_{Ri}^{(L)} = 0 \quad (L = 1, 2, 3; \ i = 1, 2, 3) \tag{22}$$

The boundary conditions, including the free surface boundary conditions, bottom boundary conditions, and the body surface conditions, for the surge, heave, and pitching oscillations, are listed as follows, respectively.

$$\begin{aligned} &\frac{\partial \phi_{Ri}^{(1)}}{\partial z} = 0 \quad (i = 1, 2, 3), \ z = h \\ &\frac{\partial^2 \phi_{Ri}^{(1)}}{\partial t^2} + \frac{\partial \phi_{Ri}^{(1)}}{\partial z} = 0 \quad (i = 1, 3), \ z = 0, \ |x| \geq a \\ &\frac{\partial \phi_{R2}^{(1)}}{\partial z} = 0 \quad z = -s, \ |x| \leq a \end{aligned} \tag{23}$$

$$\begin{aligned} &\frac{\partial \phi_{Ri}^{(2)}}{\partial z} = 0 \quad (i = 1, 2, 3), \ z = h \\ &\frac{\partial^2 \phi_{Ri}^{(2)}}{\partial t^2} + g\frac{\partial \phi_{Ri}^{(2)}}{\partial z} = 0 \quad (i = 1, 3), \ z = 0, \ |x| \geq a \\ &\frac{\partial \phi_{R2}^{(2)}}{\partial z} = 1 \quad z = -s, \ |x| \leq a \end{aligned} \tag{24}$$

$$\begin{aligned} &\frac{\partial \phi_{Ri}^{(3)}}{\partial z} = 0 \quad (i = 1, 2, 3), \ z = h \\ &\frac{\partial^2 \phi_{Ri}^{(3)}}{\partial t^2} + g\frac{\partial \phi_{Ri}^{(1)}}{\partial z} = 0 \quad (i = 1, 3), \ z = 0, \ |x| \geq a \\ &\frac{\partial \phi_{Ri}^{(3)}}{\partial n} = \mathrm{i}\omega \left[\left(z - \xi_z\right) n_x - \left(x - \xi_x\right) n_z \right] \quad \text{on body surface} \end{aligned} \tag{25}$$

where $n = (n_x, n_z)$ is the unit normal vector and (ξ_x, ξ_z) is the rotational center of the pitching oscillation. With the assumption that the rotational center is along the z axis, we can get $\xi_x = 0$.

2.3. Analytical Solutions of the Radiated Velocity Potentials. Similar to the derivation of the solutions of the diffracted velocity potentials, the application of the method of separation variables to the governing equation (22) under the boundary conditions (23), (24), and (25) yields the radiated velocity potentials as follows:

$$\phi_{R1}^{(L)} = \sum_{m=0}^{\infty} A_m^{(L)} e^{-\widetilde{k}_m(x+a)} \frac{\cos \widetilde{k}_m (z+h)}{\cos \widetilde{k}_m h} e^{-i\omega t} \tag{26}$$

$$\begin{aligned}\phi_{R2}^{(1)} &= \left(C_0^{(1)} x + E_0^{(1)}\right) e^{-i\omega t} \\ &+ \sum_{m=1}^{\infty} \left[C_m^{(1)} \frac{\cosh (r_m x)}{\cosh (r_a x)} + E_m^{(1)} \frac{\sinh (r_m x)}{\sinh (r_a x)} \right] \\ &\cdot \cos r_m (z+h) e^{-i\omega t}\end{aligned} \tag{27}$$

$$\begin{aligned}\phi_{R2}^{(2)} &= \frac{(z+h)^2 - x^2}{2(h-s)} + \left(C_0^{(2)} x + E_0^{(2)}\right) e^{-i\omega t} \\ &+ \sum_{m=1}^{\infty} \left[C_m^{(2)} \frac{\cosh (r_m x)}{\cosh (r_a x)} + E_m^{(2)} \frac{\sinh (r_m x)}{\sinh (r_a x)} \right] \\ &\cdot \cos r_m (z+h) e^{-i\omega t}\end{aligned} \tag{28}$$

$$\begin{aligned}\phi_{R2}^{(3)} &= \sum_{m=1}^{\infty} \varepsilon \cos [\gamma_m (x-a)] \cosh [\gamma_m (z+h)] \\ &+ \left(C_0^{(3)} x + E_0^{(3)}\right) e^{-i\omega t} \\ &+ \sum_{m=1}^{\infty} \left[C_m^{(3)} \frac{\cosh (r_m x)}{\cosh (r_a x)} + E_m^{(3)} \frac{\sinh (r_m x)}{\sinh (r_a x)} \right] \\ &\cdot \cos r_m (z+h) e^{-i\omega t}\end{aligned} \tag{29}$$

$$\phi_{R3}^{(L)} = \sum_{m=0}^{\infty} B_m^{(L)} e^{\widetilde{k}_m(x-a)} \frac{\cos \widetilde{k}_m (z+h)}{\cos \widetilde{k}_m h} e^{-i\omega t} \tag{30}$$

where

$$\gamma_m = \frac{m\pi}{2a} \quad (m = 1, 2, 3, \ldots) \tag{31}$$

Combining the floating body surface condition at $z = -s$, $-a \le x \le a$ and the orthogonality of $\cos[\gamma_m(x-a)]$ over the integral interval of $-a \le x \le a$, the expression of ε can be derived as

$$\varepsilon = \frac{\cos 2a\gamma_m}{\sinh [\gamma_m (h-s)] a{\gamma_m}^3} \tag{32}$$

2.4. Determination of the Unknown Coefficients That Appeared in the Solutions of Radiated Velocity Potentials. The solutions of the unknown coefficients that appeared in the radiation potentials can be again obtained by utilizing the matching conditions at $x = \pm a$ under the principle of continuous pressure and normal velocity. We have the following.

(a) Matching Conditions for the Surge-Induced Potential

$$\phi_{R2}^{(1)} = \begin{cases} \phi_{R1}^{(1)} & -h \le z \le -d, \ x = -a \\ \phi_{R3}^{(1)} & -h \le z \le -d, \ x = a \end{cases} \tag{33a}$$

$$\frac{\partial \phi_{R1}^{(1)}}{\partial x} = \begin{cases} \dfrac{\partial \phi_{R2}^{(1)}}{\partial x} & -h \le z \le -d, \ x = -a \\ 1, & -s \le z \le 0, \ x = a \end{cases} \tag{33b}$$

$$\frac{\partial \phi_{R3}^{(1)}}{\partial x} = \begin{cases} \dfrac{\partial \phi_{R2}^{(1)}}{\partial x} & -h \le z \le -d, \ x = -a \\ 1, & -s \le z \le 0, \ x = a \end{cases} \tag{33c}$$

(b) Matching Conditions for the Heave-Induced Potential

$$\phi_{R2}^{(2)} = \begin{cases} \phi_{R1}^{(2)} & -h \le z \le -d, \ x = -a \\ \phi_{R3}^{(2)} & -h \le z \le -d, \ x = a \end{cases} \tag{34a}$$

$$\frac{\partial \phi_{R1}^{(2)}}{\partial x} = \begin{cases} \dfrac{\partial \phi_{R2}^{(2)}}{\partial x} & -h \le z \le -d, \ x = -a \\ 1, & -s \le z \le 0, \ x = a \end{cases} \tag{34b}$$

$$\frac{\partial \phi_{R3}^{(2)}}{\partial x} = \begin{cases} \dfrac{\partial \phi_{R2}^{(2)}}{\partial x} & -h \le z \le -d, \ x = -a \\ 1, & -s \le z \le 0, \ x = a \end{cases} \tag{34c}$$

(c) Matching Conditions for the Pitching-Induced Potential

$$\phi_{R2}^{(3)} = \begin{cases} \phi_{R1}^{(3)} & -h \le z \le -d, \ x = -a \\ \phi_{R3}^{(3)} & -h \le z \le -d, \ x = a \end{cases} \tag{35a}$$

$$\frac{\partial \phi_{R1}^{(3)}}{\partial x} = \begin{cases} \dfrac{\partial \phi_{R2}^{(3)}}{\partial x} & -h \le z \le -d, \ x = -a \\ z - \xi_z, & -s \le z \le 0, \ x = a \end{cases} \tag{35b}$$

$$\frac{\partial \phi_{R3}^{(3)}}{\partial x} = \begin{cases} \dfrac{\partial \phi_{R2}^{(3)}}{\partial x} & -h \le z \le -d, \ x = -a \\ z - \xi_z, & -s \le z \le 0, \ x = a \end{cases} \tag{35c}$$

For the porous walls A and B at the boundaries $x = \pm a$, the condition of continuity of normal velocity for flows passing through the porous walls A and B leads to

$$\frac{\partial \phi_{R1}^{(L)}}{\partial x} = \frac{\partial \phi_{R2}^{(L)}}{\partial x} = W_A(z,t) \quad L = (1,2,3) \ -h \le z \le -d, \ x = -a \tag{36a}$$

$$\frac{\partial \phi_{R3}^{(L)}}{\partial x} = \frac{\partial \phi_{R2}^{(L)}}{\partial x} = W_B(z,t) \quad L = (1,2,3) \ -h \le z \le -d, \ x = -a \tag{36b}$$

where the porous flow velocities $W_A(z,t)$ and $W_B(z,t)$ are assumed to obey Darcy's law; that is, they are linearly proportional to the pressure difference induced by the radiated

motions across their corresponding porous wall (Chwang [11]). With the application of the linearized Bernoulli equation, we have

$$W_A(z,t) = -G_{01}\left[\frac{k_0}{\omega}\left(\frac{\partial\phi_{R1}^{(L)}}{\partial t} - \frac{\partial\phi_{R2}^{(L)}}{\partial t}\right)\right] \quad (L = 1,2,3)\ \ x = -a,\ -d \le z \le -s \tag{37a}$$

$$W_B(z,t) = -G_{02}\left[\frac{k_0}{\omega}\left(\frac{\partial\phi_{R2}^{(L)}}{\partial t} - \frac{\partial\phi_{R3}^{(L)}}{\partial t}\right)\right] \quad (L = 1,2,3)\ \ x = a,\ -d \le z \le -s \tag{37b}$$

Utilizing the orthogonality property of eigenfunctions, $\cos\widetilde{k}_n(z+h)$, for $\phi_{R1}^{(L)}$ and $\phi_{R3}^{(L)}$ $(L = 1,2,3)$ over the integral interval of $-h \le z \le 0$, the following equations can be formulated by the matching conditions of (33b), (33c), (34b), (34c), (35b), and (35c) as

$$\int_{-h}^{0}\frac{\partial\phi_{R1}^{(1)}}{\partial x}\cos\widetilde{k}_n(z+h)\,dz = \int_{-h}^{-s}\frac{\partial\phi_{R2}^{(1)}}{\partial x}\cos\widetilde{k}_n(z+h)\,dz + \int_{-s}^{0}1\cos\widetilde{k}_n(z+h)\,dz \quad (x=-a) \tag{38}$$

$$\int_{-h}^{0}\frac{\partial\phi_{R3}^{(1)}}{\partial x}\cos\widetilde{k}_n(z+h)\,dz = \int_{-h}^{-s}\frac{\partial\phi_{R2}^{(1)}}{\partial x}\cos\widetilde{k}_n(z+h)\,dz + \int_{-s}^{0}1\cos\widetilde{k}_n(z+h)\,dz \quad (x=a) \tag{39}$$

$$\int_{-h}^{0}\frac{\partial\phi_{R1}^{(2)}}{\partial x}\cos\widetilde{k}_n(z+h)\,dz = \int_{-h}^{-s}\frac{\partial\phi_{R2}^{(2)}}{\partial x}\cos\widetilde{k}_n(z+h)\,dz \quad (x=-a) \tag{40}$$

$$\int_{-h}^{0}\frac{\partial\phi_{R3}^{(2)}}{\partial x}\cos\widetilde{k}_n(z+h)\,dz = \int_{-h}^{-s}\frac{\partial\phi_{R2}^{(2)}}{\partial x}\cos\widetilde{k}_n(z+h)\,dz \quad (x=a) \tag{41}$$

$$\int_{-h}^{0}\frac{\partial\phi_{R1}^{(3)}}{\partial x}\cos\widetilde{k}_n(z+h)\,dz = \int_{-h}^{-s}\frac{\partial\phi_{R2}^{(3)}}{\partial x}\cos\widetilde{k}_n(z+h)\,dz + \int_{-s}^{0}(z-\xi_z)\cos\widetilde{k}_n(z+h)\,dz \quad (x=-a) \tag{42}$$

$$\int_{-h}^{0}\frac{\partial\phi_{R3}^{(3)}}{\partial x}\cos\widetilde{k}_n(z+h)\,dz = \int_{-h}^{-s}\frac{\partial\phi_{R2}^{(3)}}{\partial x}\cos\widetilde{k}_n(z+h)\,dz + \int_{-s}^{0}(z-\xi_z)\cos\widetilde{k}_n(z+h)\,dz \quad (x=a) \tag{43}$$

Additionally, by combining (36a), (36b), (37a), and (37b) with the matching conditions given in (33a), (34a), and (35a), respectively, and applying the orthogonality property of eigenfunctions, $\cos r_n(z+h)$, for $\phi_{R2}^{(L)}$ (L = 1, 2, 3), over the integral interval of $-h \le z \le -s$, we have

$$\int_{-h}^{-s}\phi_{R2}^{(L)}\cos r_n(z+h)\,dz = \int_{-h}^{-d}\phi_{R1}^{(L)}\cos r_n(z+h)\,dz + \int_{-d}^{-s}\widetilde{\phi}_{R1}^{(L)}\cos r_n(z+h)\,dz \quad (x=-a, L=1,2,3) \tag{44}$$

$$\int_{-h}^{-s}\phi_{R2}^{(L)}\cos r_n(z+h)\,dz = \int_{-h}^{-d}\phi_{R3}^{(L)}\cos r_n(z+h)\,dz + \int_{-d}^{-s}\widetilde{\phi}_{R3}^{(L)}\cos r_n(z+h)\,dz \quad (x=a, L=1,2,3) \tag{45}$$

where

$$\widetilde{\phi}_{R1}^{(1)} = \sum_{m=0}^{\infty}A_m^{(1)}\left(1+\frac{\widetilde{k}_m}{iG_{01}k_0}\right)\frac{\cos\widetilde{k}_m(z+h)}{\cos\widetilde{k}_m h} + \frac{1}{iG_{01}k_0} \tag{46}$$

$$\widetilde{\phi}_{R1}^{(2)} = \sum_{m=0}^{\infty}A_m^{(2)}\left(1+\frac{\widetilde{k}_m}{iG_{01}k_0}\right)\frac{\cos\widetilde{k}_m(z+h)}{\cos\widetilde{k}_m h} \tag{47}$$

$$\widetilde{\phi}_{R1}^{(3)} = \sum_{m=0}^{\infty}A_m^{(3)}\left(1+\frac{\widetilde{k}_m}{iG_{01}k_0}\right)\frac{\cos\widetilde{k}_m(z+h)}{\cos\widetilde{k}_m h} + \frac{z}{iG_{01}k_0} \tag{48}$$

$$\widetilde{\phi}_{R3}^{(1)} = \sum_{m=0}^{\infty} B_m^{(1)} \left(1 + \frac{\widetilde{k}_m}{\mathrm{i}G_{02}k_0}\right) \frac{\cos \widetilde{k}_m (z+h)}{\cos \widetilde{k}_m h} - \frac{1}{\mathrm{i}G_{02}k_0} \tag{49}$$

$$\widetilde{\phi}_{R3}^{(2)} = \sum_{m=0}^{\infty} B_m^{(2)} \left(1 - \frac{\widetilde{k}_m}{\mathrm{i}G_{02}k_0}\right) \frac{\cos \widetilde{k}_m (z+h)}{\cos \widetilde{k}_m h} \tag{50}$$

$$\widetilde{\phi}_{R3}^{(3)} = \sum_{m=0}^{\infty} B_m^{(3)} \left(1 + \frac{\widetilde{k}_m}{\mathrm{i}G_{02}k_0}\right) \frac{\cos \widetilde{k}_m (z+h)}{\cos \widetilde{k}_m h} - \frac{z}{\mathrm{i}G_{02}k_0} \tag{51}$$

Again, the summation of terms with the infinite series is approximated by a large but finite numbers of terms, e.g., a total of M terms. Then, the unknown coefficients $A_m^{(1)}, C_m^{(1)}, E_m^{(1)}, B_m^{(1)}$ $(m = 0, 1, 2, \ldots, M)$ [4(M+1) unknowns totally] can be determined by solving the 4(M+1) system of algebraic equations formulated in (38), (39), (44), and (45) (for L=1). Similarly, the unknown coefficients $A_m^{(2)}, C_m^{(2)}, E_m^{(2)}, B_m^{(2)}$ $(m = 0, 1, 2, \ldots, M)$ can be calculated from the 4(M+1) system of algebraic equations expressed in (40), (41), (44), and (45) (for L=2) while the coefficients $A_m^{(3)}, C_m^{(3)}, E_m^{(3)}, B_m^{(3)}$ $(m = 0, 1, 2, \ldots, M)$ can be evaluated by solving the 4(M+1) system of algebraic equations formulated in (42), (43), (44), and (45) (for L=3). After the determination of the above unknown coefficients, a series of engineering properties important to practical applications could be calculated, for example, the hydrodynamic coefficients and the motion induced dynamic responses of the breakwater system.

3. Exciting Forces and Hydrodynamic Coefficients

3.1. Exciting Forces. To determine the hydrodynamic coefficients related to the induced motions of the floating breakwater system, the exciting forces and moment of the combined incident and diffracted waves on the breakwater need to be computed as inputs for solving the equation of motion. By integrating the dynamic pressures with the use of the velocity potentials of incident and diffracted waves (see (7)-(9)) over the wet surface, the hydrodynamic forces along the x direction (F_{D1}) and along the z direction (F_{D2}) can be formulated, respectively, as (Qiao et al. [24])

$$\begin{aligned} F_{D1} &= \mathrm{i}\rho\omega \sum_{m=0}^{\infty} \frac{(I_m + F_m - T_m)\left[\sin \widetilde{k}_m h - \sin \widetilde{k}_m (h-d)\right]}{\widetilde{k}_m \cos \widetilde{k}_m h} \cdot e^{-\mathrm{i}\omega t} + \mathrm{i}\rho\omega * 2a(d-s) C_0 e^{-\mathrm{i}\omega t} \\ &\quad - \mathrm{i}\rho\omega \sum_{m=0}^{\infty} \frac{2E_m}{r_m} \sin r_m (h-d)\, e^{-\mathrm{i}\omega t} \end{aligned} \tag{52}$$

$$F_{D2} = \mathrm{i}\omega\rho \left[2aE_0 + 2\sum_{m=1}^{\infty} \frac{C_m}{r_m} \tanh(r_m a) \cos r_m (h-s)\right] \cdot e^{-\mathrm{i}\omega t} \tag{53}$$

Also, the wave exciting moment (F_{D3}) that is referenced to a rotational center $(0,\xi_z)$ can be derived as

$$\begin{aligned} F_{D3} &= \mathrm{i}\rho\omega \left\{ (I_m + F_m - T_m) \cdot \left[\frac{d \sin \widetilde{k}_m (h-d) - \xi_z \sin \widetilde{k}_m h + \xi_z \sin \widetilde{k}_m (h-d)}{\widetilde{k}_m \cos \widetilde{k}_m h} + \frac{\cos \widetilde{k}_m h - \cos \widetilde{k}_m (h-d)}{\widetilde{k}_m{}^2 \cos \widetilde{k}_m h} \right] \right\} \\ &\quad \cdot e^{-\mathrm{i}\omega t} + \mathrm{i}\rho\omega \left\{ aC_0 \left(d^2 - s^2\right) - \sum_{m=1}^{\infty} \frac{2E_m}{r_m} \left[d \sin r_m (h-d) + \frac{\cos r_m (h-s) - \cos r_m (h-d)}{r_m} \right] \right\} e^{-\mathrm{i}\omega t} \\ &\quad + \mathrm{i}\rho\omega \left[2aC_0 \xi_z (d-s) - \sum_{m=1}^{\infty} \frac{2E_m \xi_z}{r_m} \sin r_m (h-d) \right] \cdot e^{-\mathrm{i}\omega t} - \mathrm{i}\rho\omega \left\{ \frac{2C_0 a^3}{3} + \sum_{m=1}^{\infty} \left[\frac{2aE_m \cos r_m (h-s)}{r_m \tanh(r_m a)} - \frac{2E_m \cos r_m (h-s)}{r_m{}^2} \right] \right\} e^{-\mathrm{i}\omega t} \end{aligned} \tag{54}$$

3.2. Hydrodynamic Coefficients. The radiation forces induced by the translational and rotational motions of the floating breakwater system can be calculated from the derived radiation potentials utilizing the linearized Bernoulli equation as

$$\begin{aligned} F_{L,k} &= \mathrm{i}\rho\omega \int_{\Gamma} \Phi_{Rk}^{(L)} e^{-\mathrm{i}\omega t} n_j d\Gamma \\ &= \rho\omega^2 X_{0j} \int_{\Gamma} \phi_{Rk}^{(L)} e^{-\mathrm{i}\omega t} n_j d\Gamma \\ &= \omega^2 X_{0j} m_{L,k} e^{-\mathrm{i}\omega t} + \mathrm{i}\omega X_{0j} d_{L,k} e^{-\mathrm{i}\omega t} \end{aligned} \tag{55}$$

where $m_{L,k}$ is the radiation-induced added mass and the $d_{L,k}$ denotes the radiation damping. The expressions are, respectively,

$$m_{L,k} = \mathrm{Re}\left(\rho \int_{\Gamma} \phi_{Rk}^{(L)} n_j d\Gamma\right) = \mathrm{Re}\left(\rho \widetilde{F}_{L,k}\right) \tag{56}$$

$$d_{L,k} = \mathrm{Im}\left(\rho\omega \int_{\Gamma} \phi_{Rk}^{(L)} n_j d\Gamma\right) = \mathrm{Im}\left(\rho\omega \widetilde{F}_{L,k}\right) \tag{57}$$

$\widetilde{F}_{L,k}$ can be computed with formulations given below

$$\begin{aligned}\widetilde{F}_{1,1} &= \left(\int_{-d}^{0}\phi_{R1}^{(1)}\big|_{x=-a}\,dz - \int_{-d}^{0}\phi_{R3}^{(1)}\big|_{x=a}\,dz\right)\\ &+ \left(\int_{-d}^{-s}\phi_{R2}^{(1)}\big|_{x=-a}\,dz - \int_{-d}^{-s}\phi_{R2}^{(1)}\big|_{x=a}\,dz\right)\\ &= \sum_{m=1}^{M}\frac{A_m^{(1)}-B_m^{(1)}}{\widetilde{k}_m\cos\widetilde{k}_m h}\left[\sin\widetilde{k}_m h-\sin\widetilde{k}_m(h-d)\right]\\ &+ 2aC_0^{(1)}(d-s)+\sum_{m=1}^{M}\frac{2E_m^{(1)}}{r_m}\left[\sin m\pi\right.\\ &\left.-\sin r_m(h-d)\right]\end{aligned} \tag{58}$$

$$\begin{aligned}\widetilde{F}_{2,2} &= \int_{-a}^{a}\phi_{R2}^{(2)}\big|_{z=-x}\,dx = 2aE_0^{(2)}\\ &+\sum_{m=1}^{M}\frac{2C_m^{(2)}}{r_m}\tanh(r_m a)\cos r_m(h-s)+a(h-s)\\ &-\frac{a^3}{3(h-s)}\end{aligned} \tag{59}$$

$$\begin{aligned}\widetilde{F}_{3,3} &= \int_{-d}^{0}\left(\phi_{R1}^{(3)}\big|_{x=-a}-\phi_{R3}^{(3)}\big|_{x=a}\right)(z-\xi_z)\,dz\\ &+\int_{-d}^{-s}\left(\phi_{R2}^{(3)}\big|_{x=-a}-\phi_{R2}^{(3)}\big|_{x=a}\right)(z-\xi_z)\,dz\\ &-\int_{-a}^{a}\phi_{R2}^{(3)}\big|_{x=-s}\,x\,dx=\sum_{m=0}^{M}\left\{\left(A_m^{(3)}-B_m^{(3)}\right)\right.\\ &\cdot\left[\frac{d\sin\widetilde{k}_m(h-d)-\xi_z\sin\widetilde{k}_m(h-d)}{\widetilde{k}_m\cos\widetilde{k}_m h}\right.\\ &\left.\left.+\frac{\cos\widetilde{k}_m h-\cos\widetilde{k}_m(h-d)}{\widetilde{k}_m{}^2\cos\widetilde{k}_m h}\right]\right\}+aC_0^{(3)}\left(d^2-s^2\right)\\ &-\sum_{m=1}^{M}\frac{2E_m^{(3)}}{r_m}\left[d\sin\widetilde{k}_m(h-d)\right.\\ &\left.+\frac{\cos r_m(h-s)-\cos r_m(h-d)}{r_m}\right]+2aC_0^{(3)}\xi_z(d\\ &-s)-\sum_{m=1}^{M}\frac{2E_m^{(3)}\xi_z}{r_m}\sin r_m(h-d)-\frac{2}{3}C_0^{(3)}a^3-\sum_{m=1}^{M}\varepsilon\\ &\cdot\cosh\gamma_m(h-s)\frac{1-\cos 2a\gamma_m}{\gamma_m{}^2}+\sum_{m=1}^{M}\left\{(\varepsilon\cos m\pi\right.\\ &-\varepsilon)\left[\frac{d\sinh\gamma_m(h-d)-s\sinh\gamma_m(h-s)}{\gamma_m}\right.\\ &\left.\left.-\frac{\cosh\gamma_m(h-s)-\cosh\gamma_m(h-d)}{\gamma_m{}^2}\right]\right\}\\ &-\sum_{m=1}^{M}\frac{E_m^{(3)}\cos r_m(\mathrm{h}-\mathrm{s})}{r_m\sinh r_m a}\left(2a\cosh r_m a\right.\\ &\left.-\frac{2\sinh r_m a}{r_m}\right)\end{aligned} \tag{60}$$

$$\begin{aligned}\widetilde{F}_{3,1} &= \widetilde{F}_{1,3}=\int_{-d}^{0}\left(\phi_{R1}^{(3)}\big|_{x=-a}-\phi_{R3}^{(3)}\big|_{x=a}\right)dz\\ &+\int_{-d}^{-s}\left(\phi_{R2}^{(3)}\big|_{x=-a}-\phi_{R2}^{(3)}\big|_{x=a}\right)dz=\sum_{m=0}^{M}\left(A_m^{(3)}\right.\\ &\left.-B_m^{(3)}\right)\frac{\sin\widetilde{k}_m h-\sin\widetilde{k}_m(h-d)}{\widetilde{k}_m\cos\widetilde{k}_m h}-2(h-s)\\ &\cdot\left[\frac{a^3}{6(h-s)}+aC_0^{(3)}\right]+\frac{a(h-s)^3-a(h-d)^3}{3(h-s)}\\ &+\sum_{m=1}^{M}\frac{2E_m^{(3)}}{r_m}\sin r_m(h-d)\end{aligned} \tag{61}$$

3.3. Equation of Motion and RAOs. The derived solutions for the diffraction and radiation problems could now be integrated with the equation of motion of the floating breakwater system to analyze the dynamic responses of the structural system. We have

$$\left\{-\omega^2[M+m]-\mathrm{i}\omega[d]+[s]\right\}[X_0]=[F_0] \tag{62}$$

where $[X_0]=[X_{01},X_{02},X_{03}]^T$ and are vectors indicating the motion amplitudes and the wave exciting forces, respectively. $[m]$ and $[d]$ are added mass and damping matrices, $[M]$ is the mass matrix, and $[S]$ denotes the hydrostatic restoring force matrix; they can be expressed as

$$[M]=\begin{bmatrix}m_0 & 0 & -m_0Z_G\\ 0 & m_0 & 0\\ -m_0Z_G & 0 & 1\end{bmatrix} \tag{63}$$

$$[S]=\begin{bmatrix}0 & 0 & 0\\ 0 & 2\rho g a & 0\\ 0 & 0 & m_0 g\overline{GM}\end{bmatrix} \tag{64}$$

Here m_0 is the mass per unit length of the floating breakwater and z_G is the z-coordinate of the center of gravity. The mass moment of inertia about y-axis I can be computed by $I=m_0r_G{}^2$, in which r_G is the radius of gyration in pitching oscillation and $\overline{GM}$ is the metacentric height of the floating breakwater system. Once X_{0j} (j=1, 2, 3) are determined by solving (62), the RAOs (Response Amplitude Operators) of the breakwater system can be calculated as

$$RAO_j=\frac{X_{0j}}{H_j}\quad(j=1,2,3) \tag{65}$$

4. Results and Discussion

The validation of the wave diffraction solutions in terms of reflection/transmission coefficients and hydrodynamic loads for a train of monochromatic wave propagating through the proposed floating breakwater system that consists of a partially submerged rectangular body and with or without the attached two porous side walls has been carried out in a previous study (Qiao et al. [24]). Here, additional

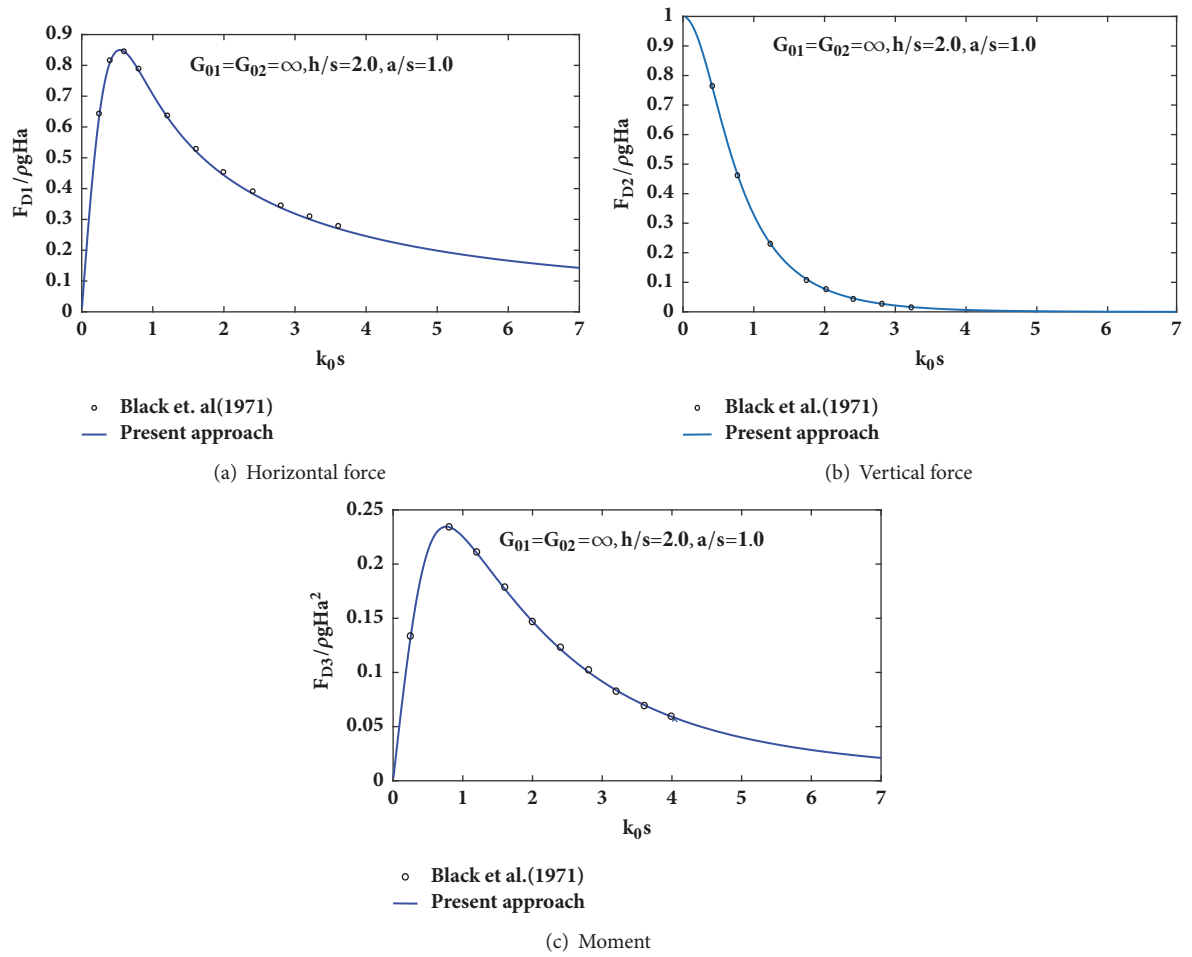

FIGURE 2: Comparison of the dimensionless wave exciting forces and moment versus $k_0 s$ for $h/s = 2.0$, $a/s = 3.0$, $G_{01} = G_{02} \longrightarrow \infty$: (a) dimensionless horizontal exciting force; (b) dimensionless vertical exciting force; (c) dimensionless exciting moment about the rotational center of $(0, 0)$.

comparisons of wave diffraction results with other published numerical solutions for the limiting case of neglecting the effect of two porous walls are again presented. For the wave radiation problem, the motion induced hydrodynamic coefficients, such as added mass and damping coefficient, are also investigated for their variations with changes of wave parameters. As a validation, those results for the cases without porous walls are compared with limited numerical solutions published in literatures. Subsequently, the effects of various dimensionless parameters, for example, porous properties, incident wave conditions, and the geometry of floating body, to wave-induced hydrodynamic forces, hydrodynamic coefficients, and RAOs were also examined. In our computations, the first 40 terms in the infinite series of the diffraction potentials and radiation potentials are taken, the same as [7]; namely, M=40.

As an example showing the results comparisons for the diffraction problem, Figure 2 illustrates the variations of the dimensionless exciting forces in horizontal and vertical directions versus dimensionless wavelength, $k_0 s$, for the case of $h/s = 2.0$, $a/s = 1.0$, $G_{01} = G_{02} \longrightarrow \infty$. The exciting moments with reference to the rotational center of (0,0) are also presented in Figure 2. Here, $G_{01} = G_{02} \longrightarrow \infty$ represents the case of a floating breakwater system without dual porous side walls. The numerical results computed by Black et al. [4] are also plotted in Figure 2. The comparisons indicate that the exciting forces and moments are well predicted by the present analytical model. Both the analytical solutions and the numerical results reveal that the horizontal exciting forces and the exciting moments show rapidly increasing trend initially until a peak value is reached and, then, are followed by a gradual decrease of the values with the further increase of $k_0 s$. However, the vertical forces as shown in Figure 2(b) decrease continuously with an increase in $k_0 s$. According to the results given in the previous study by Qiao et al. [24], it indicated that the effectiveness of the porous walls is reflected with the reduction of the vertical hydrodynamic forces and when the breakwater system is rotated with reference to the bottom center of the body, the induced moment can also be reduced. However, due to the added additional length of the porous walls, the horizontal forces are slightly greater than those without porous walls.

Figure 3 presents the variations of the dimensionless added mass and damping coefficients in surge only motion

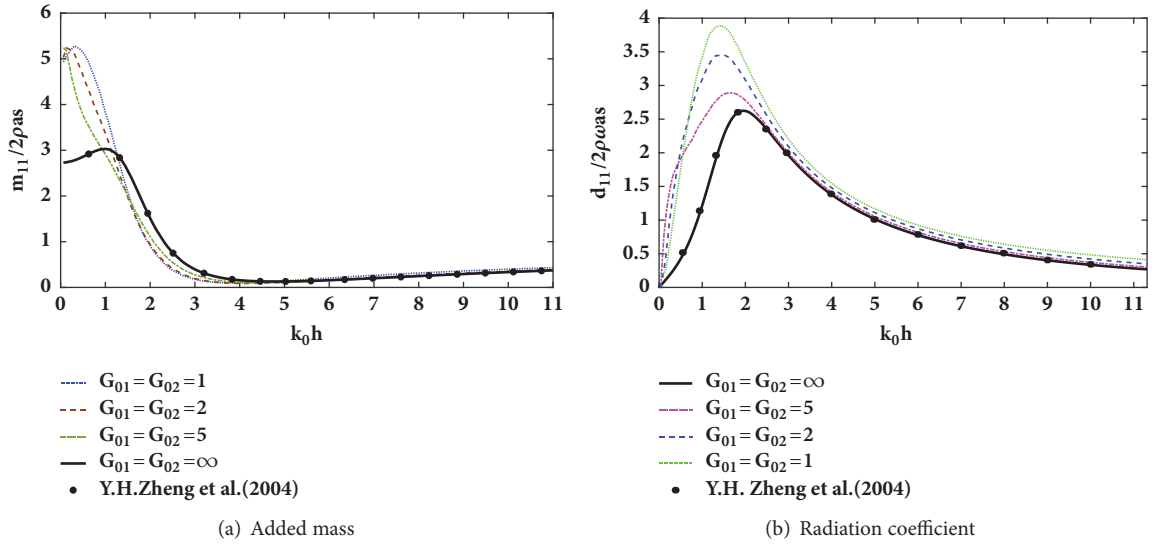

(a) Added mass (b) Radiation coefficient

FIGURE 3: Variation of the dimensionless surge-surge hydrodynamic coefficients ((a) for the added mass and (b) for the radiation damping) versus k_0h under the conditions of different porous-effect parameters for $s/h = 1/3$, $d/h = 1/2$, $a/h = 1/6$.

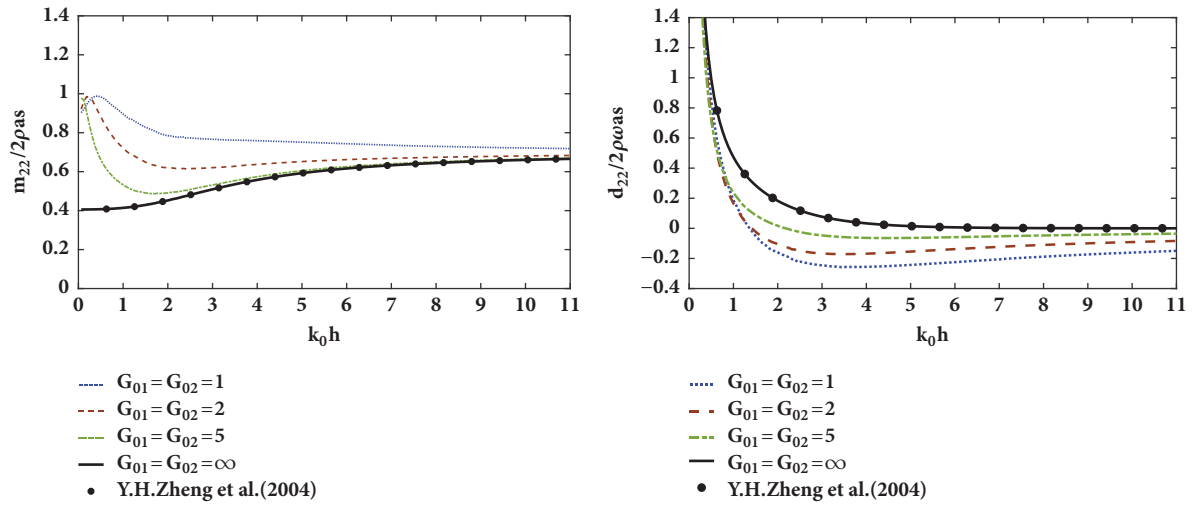

(a) Added mass (b) Radiation damping

FIGURE 4: Variation of the dimensionless heave-heave hydrodynamic coefficients ((a) for the added mass and (b) for the radiation damping) versus k_0h under the conditions of different porous-effect parameters for $s/h = 1/3$, $d/h = 1/2$, $a/h = 1/6$.

versus k_0h for the setting of $s/h = 1/3$, $d/h = 1/2$, and $a/h = 1/6$ under the conditions of various porous-effect parameters. When $G_{01} = G_{02} = \infty$, it represents the case without considering the effect of dual porous walls. The present analytical solutions for this limiting case can be adopted to compare to the limited numerical results available in the study of [7]. The comparison plot is shown in Figure 4 where the nearly identical matches between the present analytical solutions and the numerical results of [7] can be observed. The results shown in Figure 4 suggest that the addition of porous walls tends to enhance the added mass and damping coefficients. In general, with a decrease of porous effect parameter, the added mass and damping coefficients increase. For the variation of added mass coefficient, with porous walls, it can be seen that a peak value occurred at a long wave (small k_0h value) condition. However, for the radiation damping coefficient, it is shown to increase rapidly to its maximum value with an increase of k_0h; then, a gradual decrease trend is followed by a further increase of k_0h.

The dimensionless heave-heave added mass ($m_{22}/2\rho as$) and radiation damping coefficient ($d_{22}/2\rho\omega as$) versus k_0h under various G_{01} and G_{02} values for the case of $s/h = 1/3$, $d/h = 1/2$, $a/h = 1/6$ are presented in Figure 4. Under the limiting condition of $G_{01} = G_{02} = \infty$ (without porous walls), the numerical results produced by the study of [7] are also plotted for comparison. Again, good agreements between the present analytical solutions and the published numerical results can be noticed. The results in Figure 4(a)

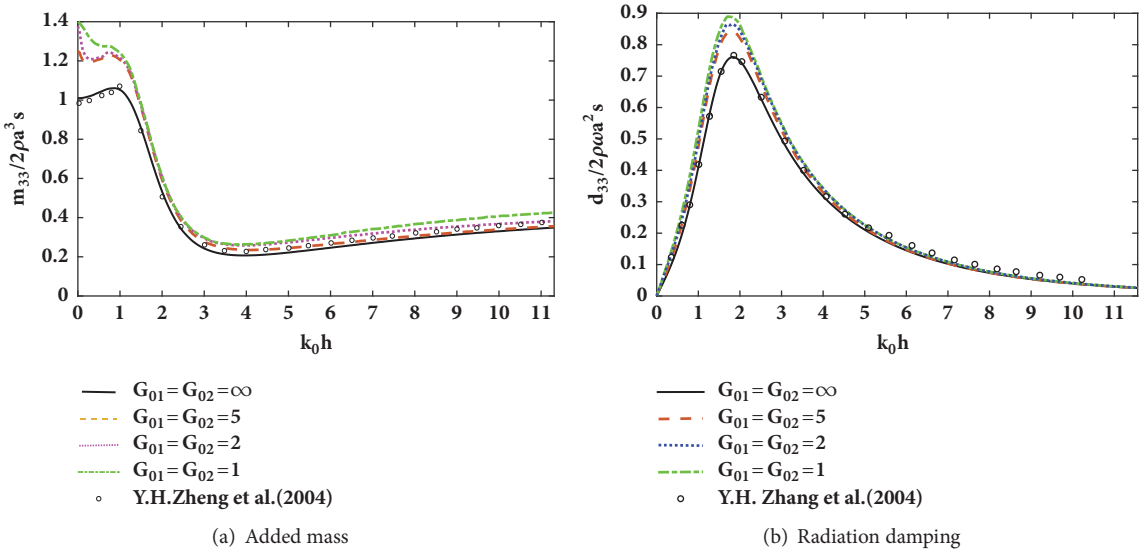

(a) Added mass (b) Radiation damping

FIGURE 5: Variation of the dimensionless pitch-pitch hydrodynamic coefficients ((a) for the added mass and (b) for the radiation damping) versus k_0h under the conditions of different porous-effect parameters for $s/h = 1/3$, $d/h = 1/2$, $a/h = 1/6$ with the rotational center set at (0, 0).

suggest that the variations of added mass for the shorter wavelength waves (large k_0h values) are less sensitive to the change of porous parameters. The presence of dual porous walls increases the heave-heave added mass, which tends to reach its maximum value at the long wave extreme. Also, a decrease in porous parameters results in an increase in heave induced added mass. As shown in Figure 4(b), the heave-heave damping coefficients decrease rapidly when k_0h increases initially. Then, a gradual changing trend is followed by a further increase in k_0h. Additionally, the presence of dual porous walls tends to reduce the values of heave-heave damping coefficients.

For the pitching induced added mass and damping coefficients, the results are plotted against k_0h in Figure 5 for various porous-effect parameters, G_{01} and G_{02}, and under the settings of $s/h = 1/3$, $d/h = 1/2$, $a/h = 1/6$. When the rotational center is set at (0,0), as shown in Figure 5, the present analytical solutions match well with the published numerical results [7] for the limiting case of no porous wall (i.e., $G_{01} = G_{02} = \infty$). It can be observed that the pitching oscillation induced added mass and damping coefficients for the floating breakwater system with dual porous side walls are greater than those without porous walls. With decrease of the porous effect parameters, the added mass and damping coefficients increase. For the added mass coefficients, it is found that the variations trends are more complex for waves with relatively smaller k_0h under the conditions of different porous-effect parameters. Generally, in cases of weaker porous-effect (for example, $G_{01} = G_{02} \leq 2$ as shown in Figure 5(a)), the value of added mass coefficient tends to approach 1.4 under the case considered. For the variations of damping coefficient as shown in Figure 5(b), the varying trends are similar to those of damping coefficient in surge motion.

The results presented in Figure 6 are the variations of the dimensionless surge-pitch added mass and damping coefficients versus k_0h for varying G_{01} and G_{02}. The case is for $s/h = 1/3$, $d/h = 1/2$, $a/h = 1/6$ with reference to the rotational center of (0,0). Clearly, the added mass and damping coefficients are shown to increase with an increase in the porous-effect parameters of both porous walls A and B, while the damping coefficients reach their absolute maximum values when k_0h is within the range of 1 and 2. The magnitude of surge-pitch hydrodynamic coefficients, especially the damping, is greatly influenced by the permeability of the dual porous walls compared to the situation with surge or pitching motion only.

The analytical solutions for the Response Amplitude Operators (RAOs) of the floating breakwater system proposed in this study are illustrated in Figure 7 as a function of dimensionless wavelength k_0h for various porous-effect parameters with the conditions of $s/h = 0.3$, $d/h = 0.5$, $a/h = 0.25$, $r_G/a = 0.9$, and $GM/a = 0.1$, where the rotational center is located at (0,0). It is found that the varying trends of surge RAOs are similar to those of pitching RAOs, although the peak values of surge RAOs are smaller than those of pitching RAOs. When the porous-effect parameters decrease, the main peak values of either surge or pitching RAOs that occurred are shifted to the wave conditions with shorter wavelength. Furthermore, for the heave RAO, it experiences a typical damped response for the case of single degree of freedom system and its maximum values of RAO would move to the lower frequency wave region when the porous-effect parameters decrease.

5. Summary and Conclusions

The hydrodynamic performance investigations, including the hydrodynamic loads, radiation induced added mass and damping coefficients, and dynamic responses related RAOs, are critical to the study that is associated with the problems of wave and structure interactions. In this study, the

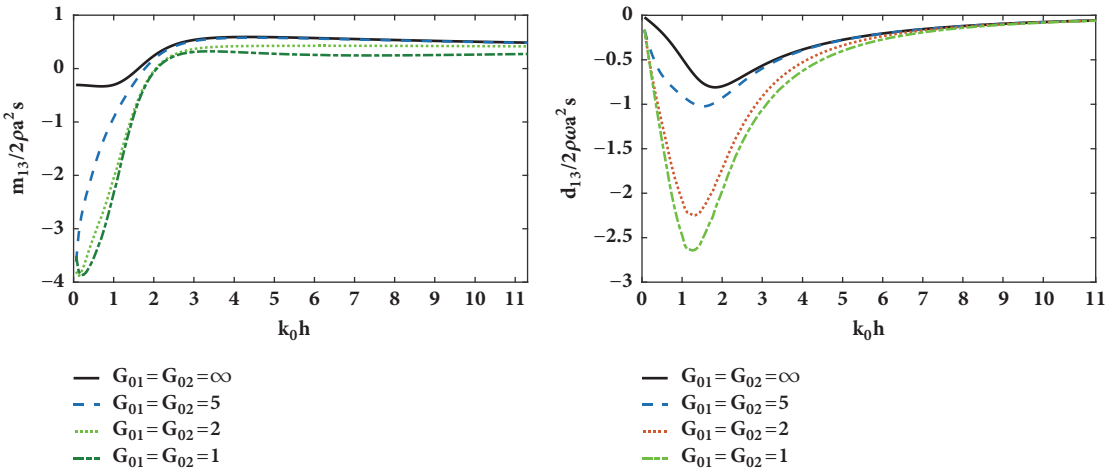

(a) Added mass (b) Radiation damping

FIGURE 6: Variation of the dimensionless surge-pitch hydrodynamic coefficients ((a) for the added mass and (b) for the radiation damping) versus k_0h under the conditions of different porous-effect parameters for $s/h = 1/3$, $d/h = 1/2$, $a/h = 1/6$ with the rotational center set at (0, 0).

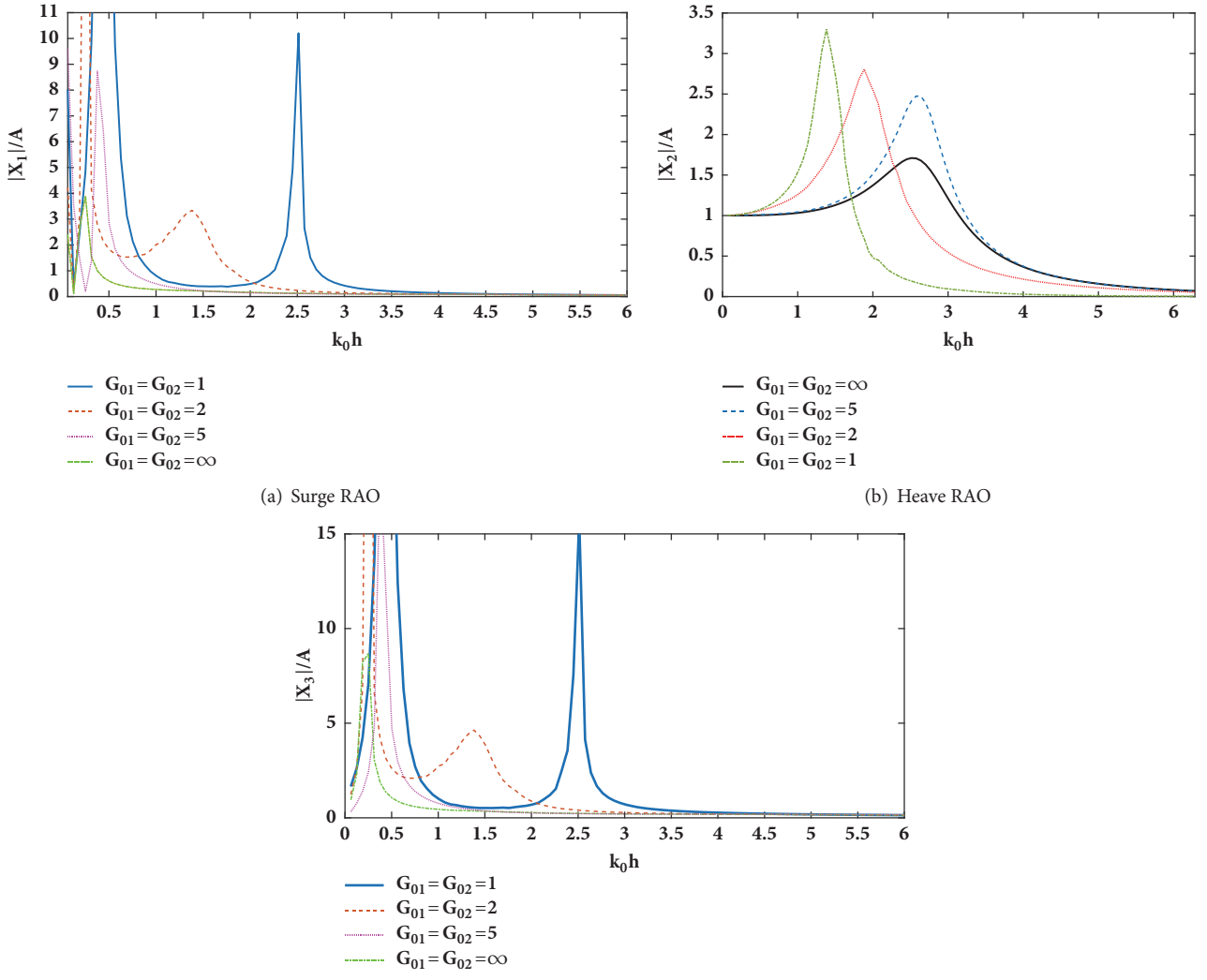

(a) Surge RAO (b) Heave RAO

(c) Pitch RAO

FIGURE 7: Variation of the dimensionless RAO ((a) for surge RAO, (b) for heave RAO, and (c) for pitch RAO) versus k_0h under the conditions of different porous-effect parameters for $s/h = 0.3$, $d/h = 0.5$, $a/h = 0.25$ $r_G/a = 0.9$, $GM/a = 0.1$ with rotation center at (0,0).

hydrodynamic problems considering a floating breakwater system that consists of a rectangular body and two vertical attached porous walls are investigated analytically based on the two-dimensional potential flow theory. The expressions of the diffraction and radiation based velocity potentials and the associated unknown coefficients for each subdomain are derived by the MEEM approach. Subsequently, the exciting hydrodynamic forces, added mass and radiation damping coefficients in terms of surge, heave and pitching motions, and the equation of motion for the floating breakwater system are formulated and calculated for various case scenarios by varying the wave conditions and porous effect parameters. Considering the limiting case without porous walls, good agreements between the present analytical solutions and published numerical results are achieved. This suggests that the present analytical model is demonstrated to be a reliable engineering tool to provide reasonable estimations for the hydrodynamic performances of a floating breakwater system with dual side porous walls. It is worthy to notice that the wave loads on the floating structures, especially the moments when referenced to the rotational center of bottom center, would be reduced with an increase in the porous-effect parameters of the porous walls. Additionally, the existence of the dual porous walls could move the peaks of surge and pitching RAOs to the waves of higher frequency when the porous effect parameters decrease. Overall, it can be concluded that a properly adopted porous-wall system when attached to a floating body can effectively improve its hydrodynamic performance as a breakwater. The analytical approach developed in this study can also be further extended to assist the theoretical analysis for other similar but improved floating breakwater systems.

Data Availability

The data used to support the findings of this study are available from the corresponding author upon request.

Conflicts of Interest

The authors declare that they have no conflicts of interest.

Acknowledgments

This work was supported by "Fundamental Research Funds for the Central Universities" (Grand No. 017180224).

References

[1] I.-H. Cho, "Transmission coefficients of a floating rectangular breakwater with porous side plates," *International Journal of Naval Architecture and Ocean Engineering*, vol. 8, no. 1, pp. 53–65, 2016.

[2] H. Hu, K.-H. Wang, and A. N. Williams, "Wave motion over a breakwater system of a horizontal plate and a vertical porous wall," *Ocean Engineering*, vol. 29, no. 4, pp. 373–386, 2001.

[3] C. C. Mei and J. L. Black, "Scattering of surface waves by rectangular obstacles in water of finite depth," *Journal of Fluid Mechanics*, vol. 38, no. 3, pp. 499–511, 1969.

[4] J. L. Black, C. C. Mei, and M. C. G. Bray, "Radiation and scattering of water waves by rigid bodies," *Journal of Fluid Mechanics*, vol. 46, no. 1, pp. 151–164, 1971.

[5] N. Drimer, Y. Agnon, and M. Stiassnie, "A simplified analytical model for a floating breakwater in water of finite depth," *Applied Ocean Research*, vol. 14, no. 1, pp. 33–41, 1992.

[6] J.-F. Lee, "On the heave radiation of a rectangular structure," *Ocean Engineering*, vol. 22, no. 1, pp. 19–34, 1995.

[7] Y. H. Zheng, Y. G. You, and Y. M. Shen, "On the radiation and diffraction of water waves by a rectangular buoy," *Ocean Engineering*, vol. 31, no. 8-9, pp. 1063–1082, 2004.

[8] E. D. Christensen, H. B. Bingham, A. P. Skou Friis, A. K. Larsen, and K. L. Jensen, "An experimental and numerical study of floating breakwaters," *Coastal Engineering Journal*, vol. 137, pp. 43–58, 2018.

[9] E. Koutandos, P. Prinos, and X. Gironella, "Floating breakwaters under regular and irregular wave forcing: Reflection and transmission characteristics," *Journal of Hydraulic Research*, vol. 43, no. 2, pp. 174–188, 2005.

[10] G. H. Dong, Y. N. Zheng, Y. C. Li, B. Teng, C. T. Guan, and D. F. Lin, "Experiments on wave transmission coefficients of floating breakwaters," *Ocean Engineering*, vol. 35, no. 8-9, pp. 931–938, 2008.

[11] A. T. Chwang, "A porous-wavemaker theory," *Journal of Fluid Mechanics*, vol. 132, pp. 395–406, 1983.

[12] Y. C. Li, Y. Liu, and B. Teng, "Porous effect parameter of thin permeable plates," *Coastal Engineering Journal*, vol. 48, no. 4, pp. 309–336, 2006.

[13] S. R. Manam and M. Sivanesan, "Scattering of water waves by vertical porous barriers: an analytical approach," *Wave Motion. An International Journal Reporting Research on Wave Phenomena*, vol. 67, pp. 89–101, 2016.

[14] A. T. Chwang and Z. Dong, "Wave-trapping due to a porous plate," in *Proceedings of 15 ONR symposium on Naval Hydrodynamics*, pp. 407–414, 1985.

[15] S. Zhu and A. T. Chwang, "Analytical study of porous wave absorber," *Journal of Engineering Mechanics*, vol. 127, no. 4, pp. 326–332, 2001.

[16] H. Behera and T. Sahoo, "Hydroelastic analysis of gravity wave interaction with submerged horizontal flexible porous plate," *Journal of Fluids and Structures*, vol. 54, pp. 643–660, 2015.

[17] T. L. Yip and A. T. Chwang, "Perforated wall breakwater with internal horizontal plate," *Journal of Engineering Mechanics*, vol. 126, no. 5, pp. 533–538, 2000.

[18] Y. Liu and H.-J. Li, "Wave scattering by dual submerged horizontal porous plates: Further results," *Ocean Engineering*, vol. 81, no. 5, pp. 158–163, 2014.

[19] I. H. Cho and M. H. Kim, "Wave absorbing system using inclined perforated plates," *Journal of Fluid Mechanics*, vol. 608, pp. 1–20, 2008.

[20] K.-H. Wang and X. Ren, "Water waves on flexible and porous breakwaters," *Journal of Engineering Mechanics*, vol. 119, no. 5, pp. 1025–1047, 1993.

[21] K. H. Wang and X. Ren, "Wave interaction with a concentric porous cylinder system," *Ocean Engineering*, vol. 21, no. 4, pp. 343–360, 1994.

[22] F. Zhao, T. Zhang, R. Wan, L. Huang, X. Wang, and W. Bao, "Hydrodynamic loads acting on a circular porous plate horizontally submerged in waves," *Ocean Engineering*, vol. 136, pp. 168–177, 2017.

[23] A. Mondal and R. Gayen, "Wave interaction with dual circular porous plates," *Journal of Marine Science and Application*, vol. 14, no. 4, pp. 366–375, 2015.

[24] W. L. Qiao, K.-H. Wang, and Y. Q. Sun, "Scattering of water waves by a floating body with two vertically attached porous walls," *Journal of Engineering Mechanics*, vol. 144, no. 2, Article ID 04017162, 2018.

[25] S. W. Twu and D. T. Lin, "On a highly effective wave absorber," *Coastal Engineering Journal*, vol. 15, no. 4, pp. 389–405, 1991.

[26] X. P. Yu, "Diffraction of water waves by porous breakwaters," *Journal of Waterway, Port, Coastal, and Ocean Engineering*, vol. 121, no. 6, pp. 275–282, 1995.

[27] I. J. Losada, M. A. Losada, and A. Baquerizo, "An analytical method to evaluate the efficiency of porous screens as wave dampers," *Applied Ocean Research*, vol. 15, no. 4, pp. 207–215, 1993.

[28] G. Besio and M. A. Losada, "Sediment transport patterns at Trafalgar offshore windfarm," *Ocean Engineering*, vol. 35, no. 7, pp. 653–665, 2008.

[29] H. Song and L. Tao, "Short-crested wave interaction with a concentric porous cylindrical structure," *Applied Ocean Research*, vol. 29, no. 4, pp. 199–209, 2007.

[30] L. Xiao, Y. Kou, L. Tao, and L. Yang, "Comparative study of hydrodynamic performances of breakwaters with double-layered perforated walls attached to ring-shaped very large floating structures," *Ocean Engineering*, vol. 111, pp. 279–291, 2016.

[31] T. L. Yip and A. T. Chwang, "Water wave control by submerged pitching porous plate," *Journal of Engineering Mechanics*, vol. 124, no. 4, pp. 428–434, 1998.